JTTEE5 7:497-504

PEER REVIEWED

Thermal Shock Characteristics of Plasma Sprayed Mullite Coatings

P. Ramaswamy, S. Seetharamu, K.B.R. Varma, and K.J. Rao

(Submitted 20 April 1998; in revised form 18 May 1998)

Commercially available mullite ($3Al_2O_3 \cdot 2SiO_2$) powders containing oxides of calcium and iron as impurities, have been made suitable for plasma spraying by using an organic binder. Stainless steel substrates covered with Ni-22Cr-10Al-1.0Y bond coat were spray coated with mullite. The 425 μm thick coatings were subjected to thermal shock cycling under burner rig conditions between 1000 and 1200 °C and less than 200 °C with holding times of 1, 5, and 30 min. While the coatings withstood as high as 1000 shock cycles without failure between 1000 and 200 °C, spallation occurred early at 120 cycles when shocked from 1200 °C. The coatings appeared to go through a process of self erosion at high temperatures resulting in loss of material. Also observed were changes attributable to melting of the silicate grains, which smooth down the surface. Oxidation of the bond coat did not appear to influence the failure. These observations were supported by detailed scanning electron microscopy and quantitative chemical composition analysis, differential thermal analysis, and surface roughness measurements.

Keywords mullite, oxidation resistant, plasma spray, thermal barrier coating, thermal shock resistance, zirconia

1. Introduction

The application of thermal barrier coatings (TBCs) to prevent degradation of metal components at high temperatures has been well documented in literature (Ref 1-4). The most prominent of the TBC materials have been zirconia (ZrO_2) based, which are known to offer the best TBC potential of improved performance in high-temperature applications such as diesel engines, gas turbines, and aircraft engines (Ref 5, 6). These coatings, however, possess a high concentration of oxygen ion vacancies, which at high temperature assist oxygen transport and the oxidation of the bond coat at the ceramic-bond coat interface. This leads to spallation of the ceramic, and such a mode of failure of the TBC is predominant when the films are thin as in gas turbines. This limitation has been overcome to a large extent by providing oxidation resistant bond coats (Ref 5). In diesel engines, however, when thicker layers of the TBC are present, even though the bond coat is not subjected to severe oxidation the ceramic layers tend to delaminate and spall after repeated thermal cycling. Extensive research is being carried out to find a suitable alternative to $8\%Y_2O_3$-ZrO_2. Refractive oxide coatings in general have been found to hold promise as TBCs. Alumina and mullite ($3Al_2O_3 \cdot 2SiO_2$) have been found to be suitable due to their reasonably low thermal conductivity and good corrosion resistance. Alumina coatings, however, are prone to thermal shock damage and are inferior to $8\%Y_2O_3$-ZrO_2 TBCs except in multilayer coatings (Ref 7). Plasma sprayed mullite ($3Al_2O_3 \cdot 2SiO_2$) coatings provide better chemical protection on silicon based ceramics, particularly in aggressive high temperature environments (Ref 8, 9). Also, mullite coatings have been found to extend the useful life of silicon carbide heat exchanger tubes otherwise prone to disintegration in corrosive environments. But, these conventionally plasma sprayed coatings tend to crack and debond on thermal cycling, which is a serious limitation to their application (Ref 8).

Mullite has been reported to contain a large amount of amorphous phase resulting from the rapid cooling of molten mullite on a cold substrate during their film fabrication (Ref 8). The amorphous phase in the coating crystallizes in a subsequent exposure to high temperature (750 to 1000 °C). The crystallization is accompanied by a volume contraction, and the associated stress causes cracking and debonding. Nevertheless, this problem has been overcome by heating the SiC substrate above the crystallization temperature during the plasma spraying (Ref 10). This procedure cannot be used on metallic substrates because they oxidize during atmospheric plasma spraying, and the subsequent ceramic coating is weakly bonded. Kokini et al. (Ref 11) have reported that mullite coatings on metallic substrates exhibit decreased surface cracking compared to a coating of 20% fully stabilized zirconia under conditions of equal heat flux and equal surface temperature. This is attributed to the decreased stress relaxation behavior of mullite. However, it is worth noting that 20% fully stabilized ZrO_2 is more prone to cracking than $8\%Y_2O_3$-ZrO_2. Decreased surface cracking has been observed in diesel engines coated with mullite.

Thus, it is becoming increasingly apparent that mullite offers itself as a potential candidate as a TBC material. This article investigates the thermal shock properties of plasma sprayed thick (425 μm) mullite coatings on steel substrates. The aspect of self erosion of the coatings at high temperatures (under burner rig test conditions) has been studied from surface roughness measurements. The microstructure of the heat affected coatings and the oxidation characteristics of the bond coat have also been studied using microscopy and chemical analyses of the top sur-

P. Ramaswamy and **S.Seetharamu,** Materials Technology Division, Central Power Research Institute, Bangalore—560 094, India; and **K.J. Rao** and **K.B.R. Varma,** Materials Research Centre, Indian Institute of Science, Bangalore—560 012, India.

face of the ceramic and the ceramic bond coat and bond-coat substrate interfaces.

2. Experimental Procedure

Commercially available mullite powder synthesized by the solid state reaction of alumina and silica powders was used for the present investigation. The starting powder was largely $3Al_2O_3{\cdot}2SiO_2$ (mullite) and only a small quantity of Al_2O_3 was present as a minor phase. CaO and Fe_2O_3 were present as impurities. These were converted into feedstock powders by the binder method (Ref 12) as they were not available commercially. Powders in the sieve range of −100 and +300 mesh have been used in the present work. The 100 to 300 mesh sizes, however, resulted in coarse powders, which were expected to result in increased roughness of coatings.

The coatings were prepared by plasma spraying the powders on stainless steel substrates (100 by 100 by 3 mm) already coated with 50 to 60 μm thick Ni-22Cr-10Al-1.0Y (AMDRY 962) bond coat. The thickness of the mullite overlayer was approximately 425 μm, and this thickness was achieved by repetitive buildup of the coatings at ~40 μm deposition per layer. The spraying was carried out without interruption of the spray process, and the coating was deposited in ten passes of the spray gun over the substrate. The stainless steel substrates were grit blasted with Al_2O_3 and degreased prior to plasma spraying. The substrate was air cooled, and the spray parameters were optimized through a process of trials to obtain uniform, thick, and well adherent coatings. Table 1 gives the plasma spray parameters used in the present studies.

Table 1 Plasma spray parameters

Argon flow rate, L/min	41
Hydrogen flow rate, L/min	14
Powder gas flow rate, L/min	3.4
Current, A	600
Voltage, V	71
Nozzle/electrode diameter, mm	6
Injector diameter, mm	1.5
Injector angle, degrees	90
Injector distance, mm	6
Powder feed rate, g/min	40
Spray distance, mm	120

The substrate was kept air cooled during spraying.

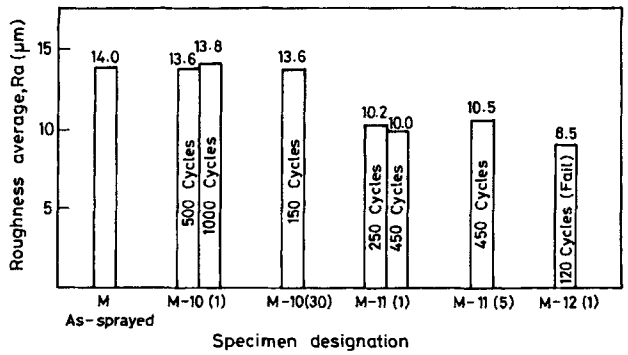

Fig. 1 Roughness average (R_a) values of Mullite coatings (as-sprayed and thermal shock cycled)

2.1 Thermal Shock Tests

The central regions of the coated surfaces were targeted in oxyacetylene flame shock cycle tests. The orifice of the gun nozzle was maintained at a distance of 100 mm from the coatings. The flame was focused such that its diameter in the central region on the ceramic surface was approximately 30 mm, and steady gas pressures were maintained to achieve the desired high temperatures (1000 to 1200 °C). The surface temperature was measured using a Pt-Pt13%Rh thermocouple. The metal substrate was not exposed to high temperature. Because the flame was perpendicular to the ceramic surface, the flow of heat was across the thickness of the ceramic coating. This ensured that oxidation of the bond coat, if any, occurred due to the flame source, focused well within the ceramic surface. The surface of the coating experienced a temperature distribution from the middle of the substrate to the edges (1000 °C ± 20 in the middle, 500 °C ± 20 at the edges). The error introduced by the thermocouple was not greater than ±5 °C. After attaining the desired maximum temperatures, the assembly was held at these temperatures for 1, 5, or 30 min. This is equivalent to subjecting the ceramic to thermal shock using the flame and soaking at the high temperatures. Subsequently the samples were suddenly withdrawn from the flame and quenched in the ambient atmosphere (without any additional source of cooling) for the same duration as was used for high temperature soaking. It was noticed that the ceramic surface attained a temperature of ~300 °C within 20 s and ~200 °C within 1 min of removal from the flame. The heat-cool cycles were continued until either the coatings peeled from the substrate or preset number of cycles were completed. The choice of various temperatures and time schedules spanned a wide range of thermal shocks and oxidation conditions. All the characterizations discussed in the subsequent sections have been carried out on the surface and the cross section of the central regions of the samples.

The affected surfaces of the thermal shock cycled specimens were evaluated for surface roughness and compared with the as-sprayed (not exposed to flame) regions of the same specimen. Surface roughness measurements were carried out using a profilometer. These surfaces were carbon coated at various stages of the thermal shock tests to study their microstructural features and any progressive damage using a scanning electron microscope (SEM). Energy dispersive x-ray analysis (EDAX) was used for quantitative chemical analysis of the surfaces and the interfaces. Phase analysis was carried out using x-ray diffractometry (XRD). Crystallinity of the specimens and phase changes, if any, of the feedstock powders, as-sprayed coatings, and some of the specimens after thermal treatments were examined using differential thermal analysis (DTA) up to 1200 °C.

3. Results and Discussion

3.1 Thermal Shock Resistance

The results of the thermal shock tests carried out on the coatings at various temperatures and for various times are indicated

in Table 2. The coatings were intact when thermal shock cycled between (a) 1000 and 200 °C (1000-200) and (b) 1100 and 200 °C (1100-200) irrespective of the duration of the heat-cool cycles. However, in the 1200 and 200 °C (1200-200) thermal shock cycling experiments, failure occurred through spallation of the ceramic coating. The coatings did not withstand more than 120 shock cycles. There was no evidence of peeling at the interface in any of the specimens subjected to thermal shock tests. This is confirmed by the presence of the ceramic coating adhering to the substrate surface in the region where failure had occurred. It is quite likely that failure occurred by the detachment of few layers of the ceramic coating, which had formed layer by layer during each pass of the plasma spray process. It was clearly a failure of the cohesion away from the interface within the ceramic layer. This result indicates that bond coat oxidation is unlikely to be the cause for spallation of the ceramic in the 1200-200 shock cycle. It is probable that fluctuations in the flame temperature and presence of impurities give rise to hot spots and local melting. The molten portions may be partly blown off by the pressure of the flame gases causing the observed spallation effects. The specimen shock cycled at lower temperatures did not exhibit any kind of failure.

3.2 Surface Roughness Measurements

All the specimens thermal shock cycled at various temperatures and durations were subjected to surface roughness measurements. The aim of the tests was to determine if the roughness average (R_a) values on the affected zone would suggest any surface degradation. Further, the possibility of the progressive damage caused to the surface at various stages of the thermal shock test can also be explored. The R_a value of the as-sprayed surface was high and measured to be 14 to 16 μm because the particle sizes of the feedstock powders were spread over 100 to 300 mesh. The R_a values of ZrO_2 coatings obtained under similar conditions (unpublished work) made using particles in the range 170 to 300 mesh size were no higher than 5 to 8 μm and were very similar to those of ZrO_2-based commercial coatings. Figure 1 shows the R_a values at the central region of the coatings where the flame had been focused during the thermal shock tests. The data pertaining to the measurements carried out at various stages of experimentation indicate that considerable smoothing down of the heat affected surfaces occurs when the coatings were exposed to 1100 °C and above. The smoothing down appears to occur within a few tens of thermal shock cycles from the start of the cycling. The heat affected zone of sample M-11(1) after 450 cycles does not exhibit further smoothing down than that shown by sample M-11(1) after 250 cycles. However, the failed region in sample M-12(1) from where the coating has spalled exhibited a greater degree of surface smoothness than any other region. This was expected because of the higher temperature of the test and the higher degree of damage causing local melting. Negligible changes occur in the R_a values of the specimens subjected to 1000-200 shock cycling. It should be noted that the maximum temperatures encountered by the coated surfaces of the diesel engine components do not extend beyond 800 °C. The use of mullite coatings for diesel engine applications has been demonstrated by Yonushonis (Ref 13). Thus,

Table 2 Thermal shock resistance test results

Sl No.	Designation	Details of the test	Maximum No. of shock cycles	Remarks
1	M	As-sprayed	...	...
2	M-10(1)	1000 °C/1 min heating	1000	Test stopped, coating intact
3	M-10(30)	1000 °C/30 min heating	150	Test stopped, coating intact
4	M-11(1)	1100 °C/1 min heating	450	Test stopped, coating intact
5	M-11(5)	1100 °C/5 min heating	450	Test stopped, coating intact
6	M-12(1)	1200 °C/1 min heating	120	Cohesive failure of ceramic overlayer; interface intact

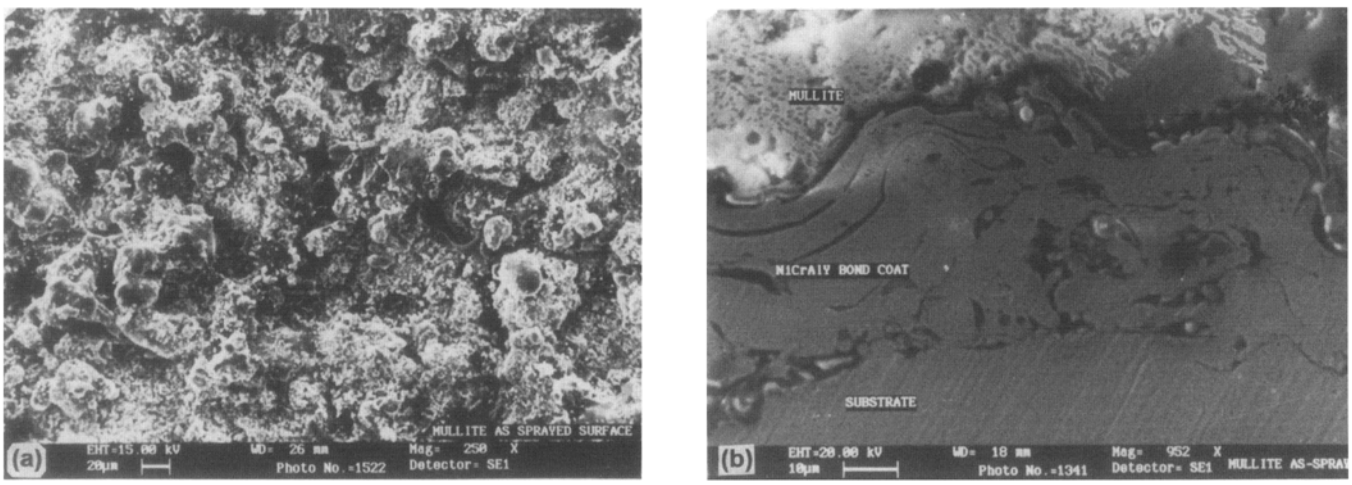

Fig. 2 Scanning electron micrographs of (a) surface and (b) cross-section of as-sprayed mullite coating. (Art has been reduced to 74% of its original size for printing.)

mullite coatings obtained by spraying powders prepared by the present method of using organic binders (Ref 12) may also be suitable candidates for improving the engine life and performance because of its good thermal shock resistance at <1000 °C and the ability to resist high temperature erosion under thermal stresses.

3.3 Microstructural Analysis

Figure 2 shows the scanning electron micrographs of the (a) surface and (b) cross section of the as-sprayed mullite (M) coating. The surface of the coating is rough, in agreement with the results of R_a measurements, and exhibits many protrusions, pores, and smooth curvatures (glassy, beadlike). Such unevenness on the surface is not typical of plasma spray coated specimens, and the presence of the rough surface in the present coating has been attributed to the coarse nature of the sprayable powder. The cross section (Fig. 2b), however, indicates a smooth interface at the substrate bond-coat ceramic junctions and suggests good adherence to each other. Figure 3 shows the scanning electron micrographs of the surfaces of (a) M-10(30) after 150 cycles and (b) M-11(5) after 250 cycles. They are compared to that of the surface of M except that it is less porous, which is attributable to a greater degree of sintering that occurs during the long duration (30 min heating cycle) of exposure to high temperature (1000 °C or more). No macro- or microcracks were observed in the ceramic overlayer. Thermal shock does not appear to play any role in material removal from the surface. Large and wide cavities are seen on the surface of M-11(5) after 250 cycles (Fig. 3b). The presence of spherical particles and smooth surfaces are suggestive of melting occurring in the region. Figure 4 presents a closer view of the region. Material removal seems to occur due to the blast pressure associated with the gas flame, which forces the molten particle to be blown off the surface. Figure 5 is a micrograph of the mounted and polished cross section of (a) the interface region and (b) the ceramic over layer of M-10(30) at the end of 150 cycles. The interface was clearly intact, devoid of any irregularities, and the ceramic, the bond coat, and the substrate appeared well bonded at the interfaces. No evidence of detachment of layers due to oxidation of the bond coat was present. Further, no macro cracks were seen in the polished ceramic over layer (Fig. 5b), indicating that the ceramic had not deformed under the thermal shock conditions.

Figure 6(a) shows the scanning electron micrograph of the failed region in M-12(1) after 120 cycles, from which the layers of ceramics flaked off indicating definite failure of only the ceramic overlayer. An enlarged view of the same region is shown in Fig. 6(b). The temperature of 1100 °C was, however, not sufficient for the ceramic to completely peel from the bond coat layer in the experiments. Figure 7 shows the EDAX spectrum of the (a) coated surface of M and (b) bond coat region in the cross section of polished sample of M. The chemical composition determined by quantitative EDAX analysis is shown in the inset of the spectrum. The as-sprayed coatings contain 70 to 75% Al_2O_3 and 25 to 30% SiO_2 (typical of $3Al_2O_3{\cdot}2SiO_2$ composition) with CaO and Fe_2O_3 impurities ranging between 1 and 3%. The bond coat has the typical composition of Ni-22Cr-10Al-1.0Y (AMDRY 962) with a small amount of oxygen (mass fraction 3 to 5%). Slight oxidation of the bond coat is expected because the plasma spraying process was not carried out in vacuum.

The as-sprayed coatings occasionally contained discrete grains of silica-rich composition, and a typical region is shown

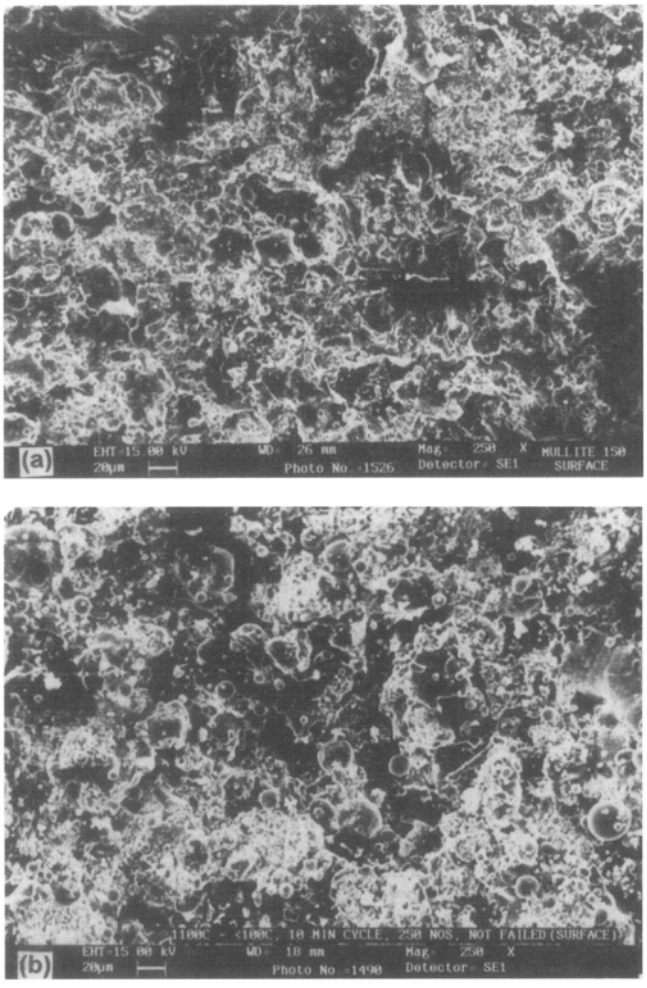

Fig. 3 Scanning electron micrographs of (a) after 150 M-10(30) and (b) M-11(5) after 250 shock cycles. (Art has been reduced to 74% of its original size for printing.)

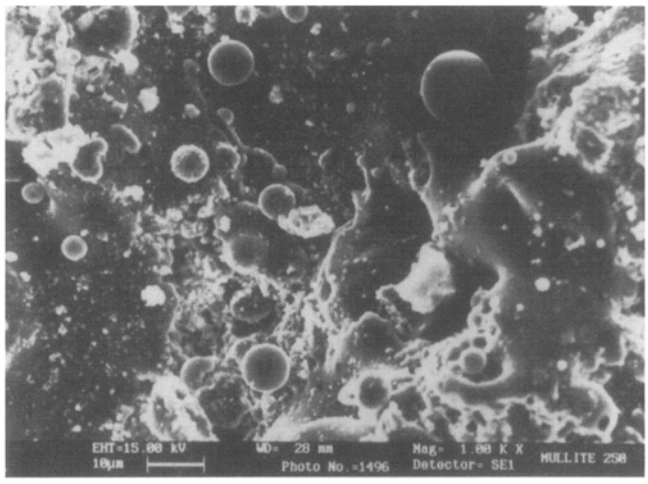

Fig. 4 Scanning electron micrograph of M-11(5) after 250 shock cycles (enlarged view). (Art has been reduced to 74% of its original size for printing.)

in the scanning electron micrograph of Fig. 8. Detailed microstructural analysis of as-sprayed specimen also revealed the presence of spherical globules similar to those observed in the thermal shock cycled specimens. The chemical compositions of the spherical globules found on the surfaces of the thermal shock cycled specimens were, however, significantly different from that of mullite. Figure 9 shows a typical EDAX spectrum from such a region in M-11(1) after 250 thermal shock cycles along with the compositional data (inset). The spherical globules contain larger amounts of SiO_2 (40 to 45%) and either CaO and/or Fe_2O_3 as impurities (5 to 15%) and correspond roughly to the formula $Al_2O_3 \cdot SiO_2$. These silica-rich grains must have a lower melting point compared to mullite grains and are, therefore, separated from the matrix. In order to study the interface and oxidation characteristics of M-10(30), the polished cross section at the region where the flame was focused was analyzed by SEM and EDAX. The elemental percentage of oxygen on the bond coat area close to the ceramic over layer was only ~8% (which is nominal), indicating that the bond coat had not oxidized significantly during thermal cycling (for 75 cumulative h). It is to be noted that the coating from the ZrO_2-CeO_2-CaO system (Ref 14), which underwent an identical test for 90 cycles (45 cumulative h), exhibited elemental oxygen in the bond coat (close to the ceramic layer) of about 15%. This suggests that mullite coatings are more beneficial than a ZrO_2 based top coat. Energy dispersive x-ray analysis of the M-10(30) surface and the bond coat at the ceramic bond-coat interface did not exhibit any unusual difference in composition from that of the as-sprayed specimen, thereby confirming the suitability of the coating for TBC application at ~1000 °C.

3.4 Phase Analysis

Figure 10 shows the XRD patterns of the sprayable mullite powder, as-sprayed mullite coatings, and heat-treated mullite coating. The patterns in Fig. 10(a) and (b) reveal the presence of $3Al_2O_3 \cdot 2SiO_2$ as the major phase and α-Al_2O_3 as the minor phase. A few small peaks in Fig. 10(b) were unidentifiable. But from the known impurities in the system, it is suspected that they may be due to either $CaAl_2SiO_6$ or $Ca_2(Fe,Mg,Ti)_6(Si,Al)_6O_{20}$. However, confirmation was not possible, both because the peaks were of low intensity and some of the peaks overlap with the major mullite and/or alumina peaks. The crystallinity of the material is evident from the fairly sharp diffraction peaks.

Glassy mullite is expected to form in the plasma sprayed specimen when molten drops of mullite are quenched on the

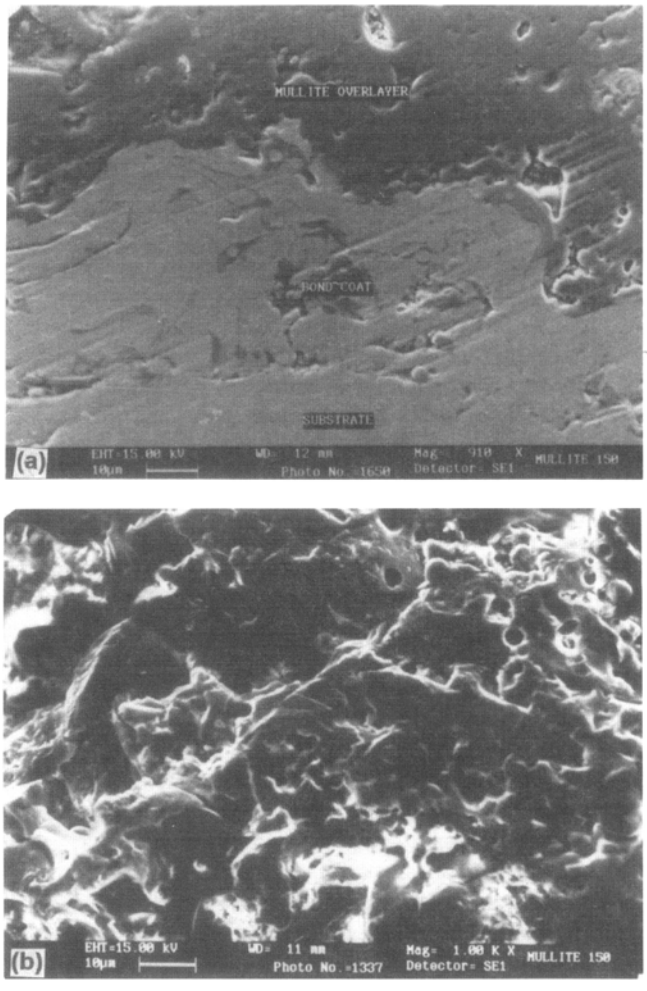

Fig. 5 Scanning electron micrographs of cross section of (a) interface region and (b) ceramic overlayer region of M-10(30) after 150 shock cycles. (Art has been reduced to 74% of its original size for printing.)

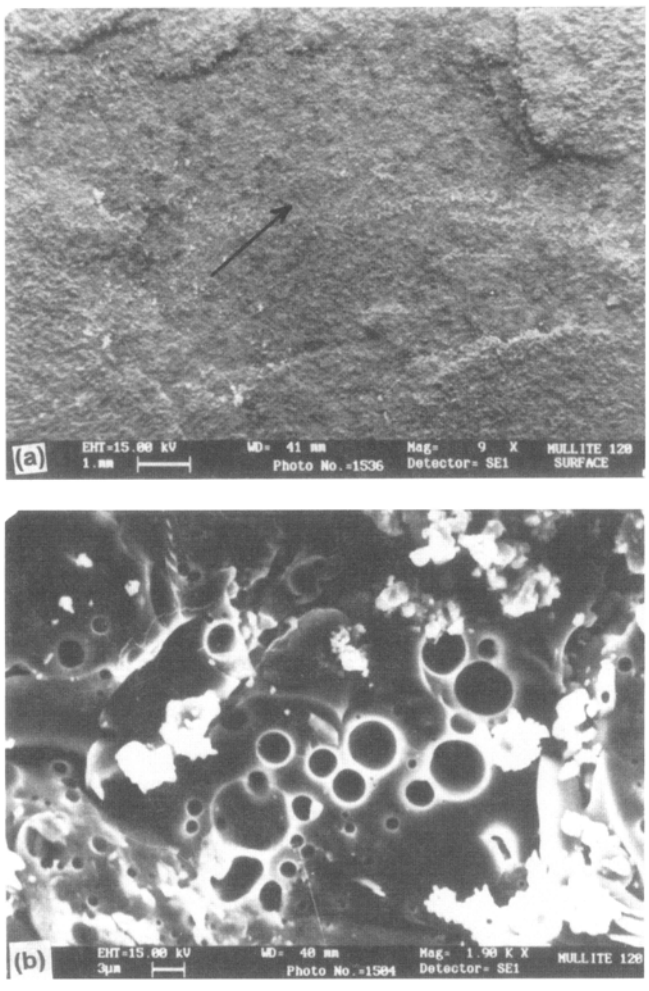

Fig. 6 Scanning electron micrograph of the (a) failed region in M-12(1) after 120 shock cycles (b) enlarged view of marked area in (a). (Art has been reduced to 74% of its original size for printing.)

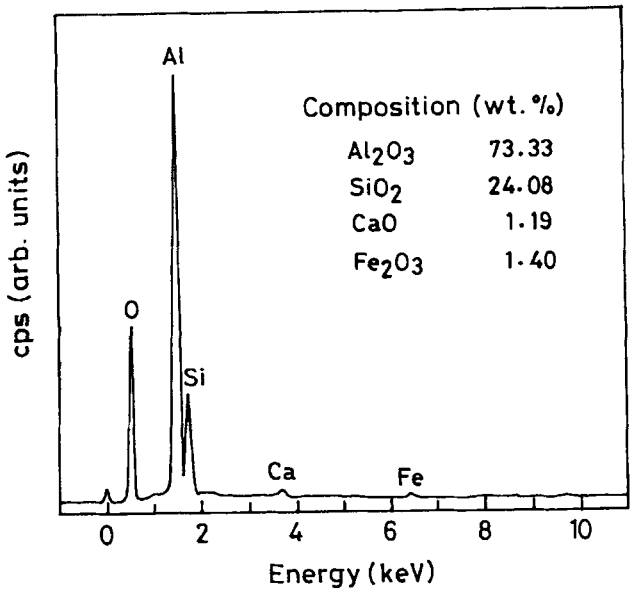

(a)

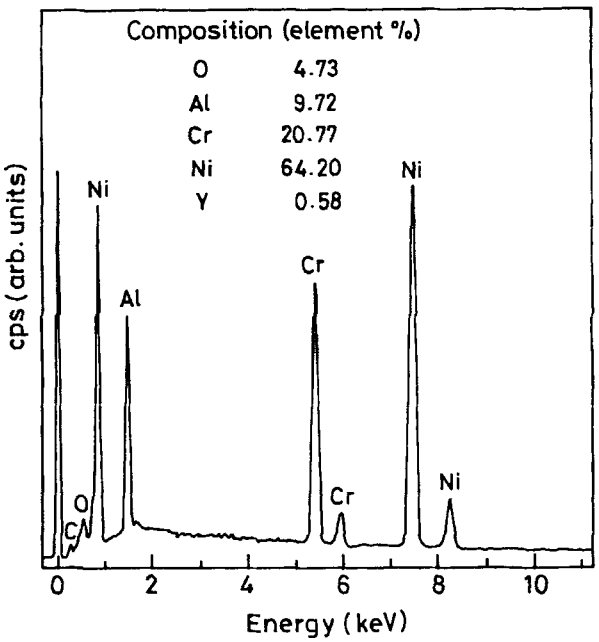

(b)

Fig. 7 Energy dispersive x-ray analysis spectrum of mullite coatings (a) as-sprayed ceramic surface and (b) bond coat region in cross section. Chemical composition is shown in inset.

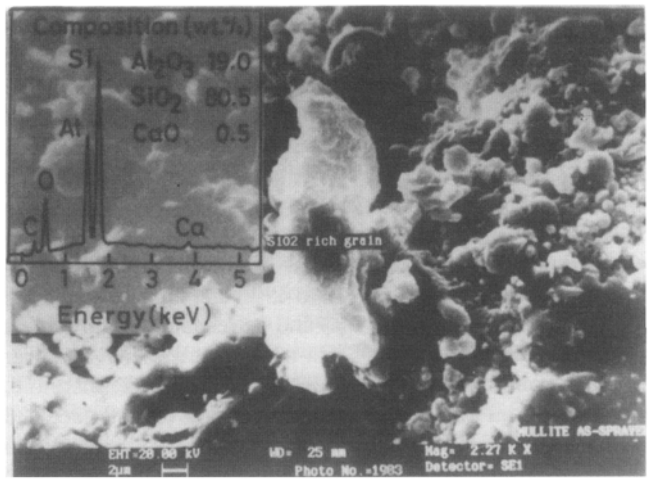

Fig. 8 Scanning electron micrograph of as-sprayed mullite coating showing SiO_2-rich grain. Energy dispersive x-ray analysis spectrum and chemical composition of the grain are shown as inset. (Art has been reduced to 74% of its original size for printing.)

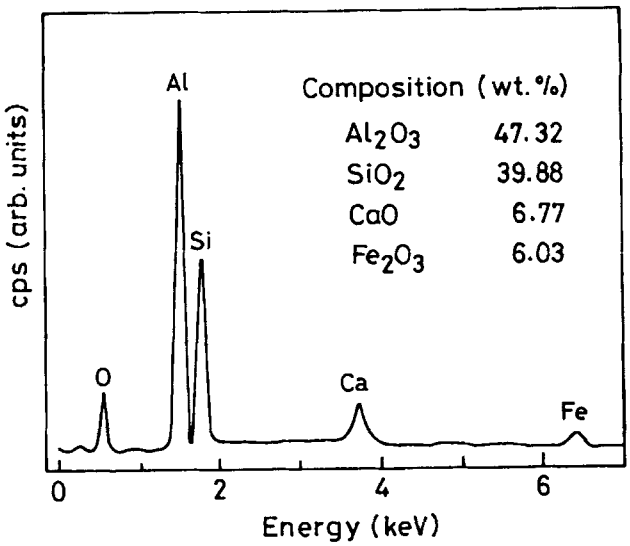

Fig. 9 Energy dispersive x-ray analysis spectrum and chemical composition (inset) of spherical globules on the surface of M-11(1) after 250 shock cycles

cold substrate (Ref 8). Formation of a glassy phase is weakly evidenced in the general shape of the background in the XRD, which is suggestive of a broad glassy diffraction peak at low values of 2θ. The authors note here that the substrate was air cooled, and it reached a temperature of approximately 200 °C during the process. The coating was removed from the substrate and was heat treated at 1025 °C for 8 h and furnace cooled. Figure 10(c) shows the XRD pattern of this sample. A significant reduction in Al_2O_3 peak intensities was observed compared to the same in 10(a) or (b), which suggests that the free Al_2O_3 and SiO_2 present in the coating have reacted during heat treatment. Peaks pertaining to free silica (quartz or crystoballite) were however not seen in the as-sprayed coating (Fig. 10b). The absence of XRD signature of SiO_2 may be either due to a low relative proportion in the sample or due to it being present in a glassy state.

3.5 Differential Thermal Analysis

Figure 11 shows the differential thermal analysis (DTA) curves obtained for sprayable powder, sample M, and sample M-10(30). The DTA curve of the product of sample M-10(30) shown in Fig. 11(c) is also included in the same figure (c′). While the thermogram of the sprayable powder (Fig. 11a) shows total absence of any exothermic or endothermic peak, both samples M and M-10(30) exhibit an exotherm around 970 °C. Similar behavior has been observed by Lee et al. (Ref 8) in their as-sprayed mullite coatings, and the presence of the peak was

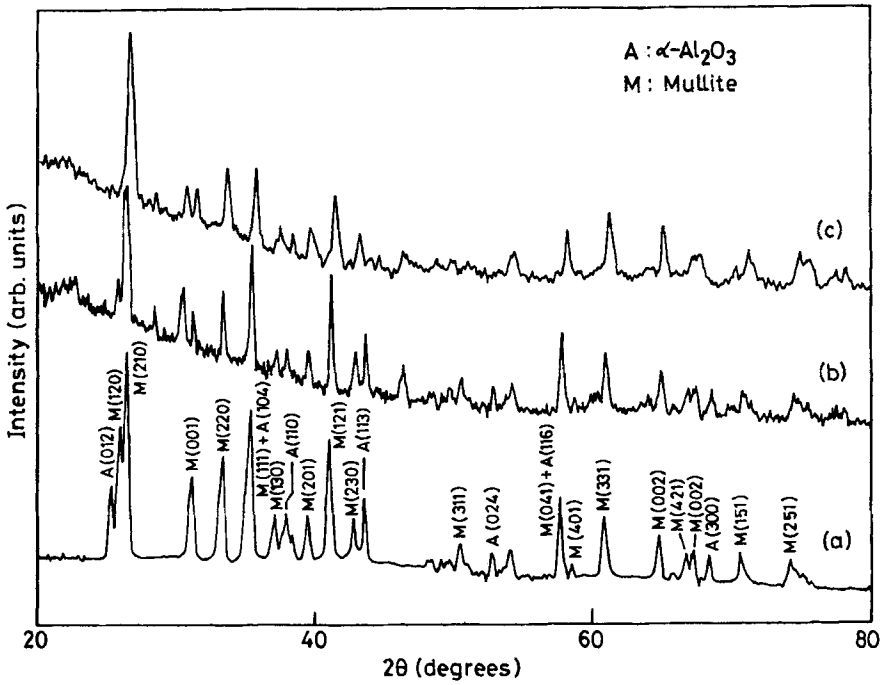

Fig. 10 X-ray diffraction patterns of (a) sprayable mullite powder, (b) as-sprayed mullite coating, and (c) mullite coatings—heat treated at 1025 °C for 8 h

attributed to the crystallization of amorphous mullite. In the present studies, both as-sprayed and all the thermally cycled specimen (including sample M-12(1), thermal cycled from 1200 °C) exhibited the endothermic phase transformation between 967 and 971 °C. It is, therefore, quite strange why thermal cycling does not eliminate this exotherm. In the literature this exotherm, which is featured in other mullitic systems, has been attributed to crystallization of glassy mullite.

This explanation is only partial in the present case because of the following observations. Although the exotherm at ~970 °C is both sharp and irreversible and quite like the exotherm due to glass-crystal transformation, it is also associated with simultaneous disappearance of diffraction peaks attributable to α-Al_2O_3, which is present in all coatings (shock cycled or otherwise) not subjected to DTA. Therefore, there is a small amount of a glassy phase that crystallizes, but it is similar to a silica and not mullite. This is possible in view of the known features in the phase diagram of Al_2O_3-SiO_2 system (Ref 15). During the plasma spray process when mullite excurses a very high temperature regime, isolated regions of molten semisilicas (SiO_2-rich aluminosilicates) are formed, which are quenched into the glassy phase. This glassy phase has a temperature window for rapid exothermic crystallization, which in shock cycling experiments is rapidly bypassed. Therefore, both the glassy phase and the minor Al_2O_3 phase are left undisturbed. But, during the relatively slow DTA experiment, rapid crystallization occurs in the temperature region. This phase transition (Hedvall effect) (Ref 16) is coupled with exothermicity, which will enable reaction between free Al_2O_3 and the silicalike phase to produce mullite that may not be identical in composition and in structure (a defective mullite) to the parent mullite. It is tempting to associate the disappearance of the split feature of the major peaks (120) and (210) of mullite in Fig. 10(c) at d =3.43 and 3.39 Å with the formation of this new mullite phase. However, further work is necessary to understand the detailed mechanism by which these two processes (disappearance of Al_2O_3 in XRD and exotherm in DTA) occur.

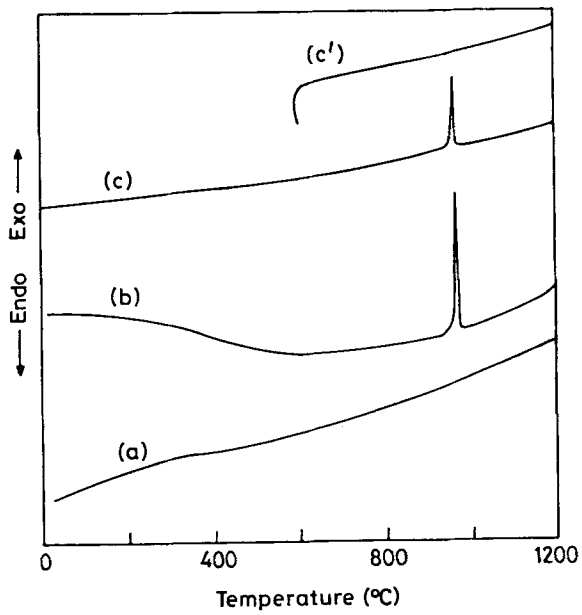

Fig. 11 Differential thermograms obtained for (a) mullite sprayable powder, (b) as-sprayed mullite coating, (c) M-10(30) after 150 shock cycles, and (c′) product of M-10(30) after differential thermal analysis

The mullite powders have also been plasma spray coated on the piston, cylinder head, and valves of a 5 hp diesel engine. The

performance of the engine is currently being studied under severe and accelerated cyclic load conditions. The coatings have successfully withstood 300 h of performance test without showing any indications of failure. Details of the investigations will be reported elsewhere.

4. Conclusions

Plasma sprayed mullite coatings were subjected to repeated thermal shock conditions from various temperatures (1000 to 1200 °C) for different durations. The coatings exhibited excellent stability when shocked from 1000 °C and withstood more than 1000 cycles without failure. The cycling imparted no further oxidation to the bond coat from the as-sprayed condition, thereby indicating the favorable response of the material as a thermal barrier coating. The shock cycling from higher temperatures (1200 °C), however, has resulted in the formation of molten regions and subsequent removal of the material. The coatings also have minor amounts of glassy phase of silica-rich composition, which exhibits crystallization and chemical reaction during annealing. This has been attributed to the considerably high surface roughness of the coatings, which occurs because some regions on the coating experience much higher temperature and therefore melt.

Acknowledgment

The authors thank the management of IISc. and CPRI for the interest shown in this work. Gratitude is also due to referees for their valuable comments.

References

1. N. Carlson and B.L. Stoner, "Thermal Barrier Coating on High Temperature Industrial Gas Turbine Engines," NASA CR-135147, Feb 1977
2. R.A. Miller and C.C. Berndt, Performance of Thermal Barrier Coatings in High Heat Flux Environments, *Thin Solid Films,* Vol 119, 1984, p 195-202
3. J.T. DeMasi-Marcin and D.K. Gupta, Protective Coatings in the Gas Turbine Engine, *Surf. Coat. Technol.,* Vol 68/69, 1994, p 1-9
4. A. Maricocchi, A. Bartz, and D. Wortman, PVD Experience on GE Aircraft Engine, *J. Therm. Spray Technol.,* Vol 6 (No. 2), 1997, p 193-198
5. A. Bennett, Properties of Thermal Barrier Coatings, *Mater. Sci. Technol.,* Vol 2, March 1986, p 257-261
6. P. Vincenzini, Zirconia Thermal Barrier Coatings for Engine Applications, *Ind. Ceram.,* Vol 10 (No. 3), 1990, p 113-126
7. P. Ramaswamy, S. Seetharamu, K.B.R. Varma, and K.J. Rao, Al_2O_3-ZrO_2 Composite Coatings For Thermal Barrier Applications, *Compos. Sci. Technol.,* Vol 57, 1997, p 81-89
8. K.N. Lee, R.A. Miller, and N.S. Jacobson, New Generation of Plasma Sprayed Mullite Coatings on Silicon Carbide, *J. Am. Ceram. Soc.,* Vol 78 (No. 3), 1995, p 705-710
9. D.P. Butt, J.J. Mecholsky, Jr., M. Van Roode, and J.R. Price, Effects of Plasma Sprayed Distribution of Silicon Carbide Materials, *J. Am. Ceram. Soc.,* Vol 73 (No. 9), 1996, p 2690-2696
10. K.N. Lee and R.A. Miller, Oxidation Behavior of Mullite-Coated SiC and SiC/SiC Composites under Thermal Cycling between Room Temperature and 1200 °C-1400 °C, *J. Am. Ceram. Soc.,* Vol 79 (No. 3), 1996, p 620-626
11. K. Kokini, Y.R. Takeuchi, and B.D. Choules, Surface Thermal Cracking of Thermal Barrier Coatings Owing to Stress Relaxation: Zirconia vs. Mullite, *Surf. Coat. Technol.,* Vol 82, 1996, p 77-82
12. P. Ramaswamy, S. Seetharamu, K.B.R. Varma, and K.J. Rao, A Simple Method for the Preparation of Plasma Sprayable Powders Based on ZrO_2, *J. Mater. Sci.,* Vol 31, 1996, p 6325-6332
13. T. Yonushonis, "Ceramic Thermal Barrier Coating for Rapid Thermal Cycling Applications," U.S. Patent No. 5,320,909, 14 June 1994
14. P. Ramaswamy, S. Seetharamu, K.B.R. Varma, and K.J. Rao, Evaluation of CaO-CeO_2-Partially Stabilized Zirconia Thermal Barrier Coatings, accepted for print in *Ceram. Int.*
15. H. Schneider, K. Okada, and J. Pask, *Mullite and Mullite Ceramics,* Chapter 3, John Wiley & Sons, p 83-104
16. C.N.R. Rao and K.J. Rao, *Phase Transitions in Solids,* Chapter 1, McGraw-Hill International, 1979